Dual-encapsulated highly conductive and liquid-free phase change composites enabled by polyurethane/graphite nanoplatelets networks for efficient energy storage and thermal management

Minqiang Wu[1,‡], *Tingxian Li*[1,‡,*], *Pengfei Wang*[1], *Si Wu*[1], *Taishen Yan*[1], *Jiaxing Xu*[1], *Ruzhu Wang*[1,*], *Jie Lin*[2]

[1] Research Center of Solar Power & Refrigeration, School of Mechanical Engineering, Shanghai Jiao Tong University, Shanghai, 200240, China

[2] Department of Engineering Science, University of Oxford, Parks Road, Oxford OX1 3PJ, United Kingdom

[‡] These authors contributed equally to this work.

* Correspondence and requests for materials should be addressed to T.X. Li (email: Litx@sjtu.edu.cn) or to R.Z. Wang (email: Rzwang@sjtu.edu.cn).

ABSTRACT

Thermal management based on phase change materials (PCMs) has attracted tremendous attention for the passive cooling and preheating of electronic devices. However, the widespread utilization of PCM-based thermal management is always restricted by the low thermal conductivity and liquid leakage of melted PCMs. Herein, we report a dual-encapsulation strategy to fabricate highly conductive and liquid-free polyethylene glycol (PEG)-based phase change composites (PCCs) for energy storage and thermal management. The PEG is firstly infiltrated into the cross-linked network of polyurethane (PU) to synthesize hybridized semi-interpenetrated composites (PEG@PU), and then the composites are incorporated with an aligned reticulated graphite nanoplatelets (RGNPs) *via* pressure-induced assembly to fabricate highly conductive PCCs (PEG@PU-RGNPs). The dual-encapsulation networks of PU and RGNPs enable the PCCs to show excellent mechanical strength, liquid-free phase change, and stable thermal properties. More importantly, contributed by the RGNPs networks as thermal/electrical transport pathways, the PCCs exhibit high thermal conductivity up to 27.0 W m^{-1} K^{-1} and electrical conductivity of 51.0 S cm^{-1}, superior to the state-of-the-art PEG-based PCCs. Furthermore, we demonstrate the PCC-based battery thermal management (BTM) toward the versatile demands of passive cooling at high temperatures and active preheating at low temperatures. The PCC-based BTM realizes battery warm-up with a temperature range of 34-40 ^{o}C at an ambient temperature of 0 ^{o}C, and battery cooling with a controllable temperature below 55 ^{o}C even at a hot environment (35 ^{o}C) during continuous high-rate charging/discharging cycles. Therefore, our work provides a promising route for fabricating highly conductive and liquid-free PCCs toward efficient energy storage and thermal management.

TOC GRAPHICS

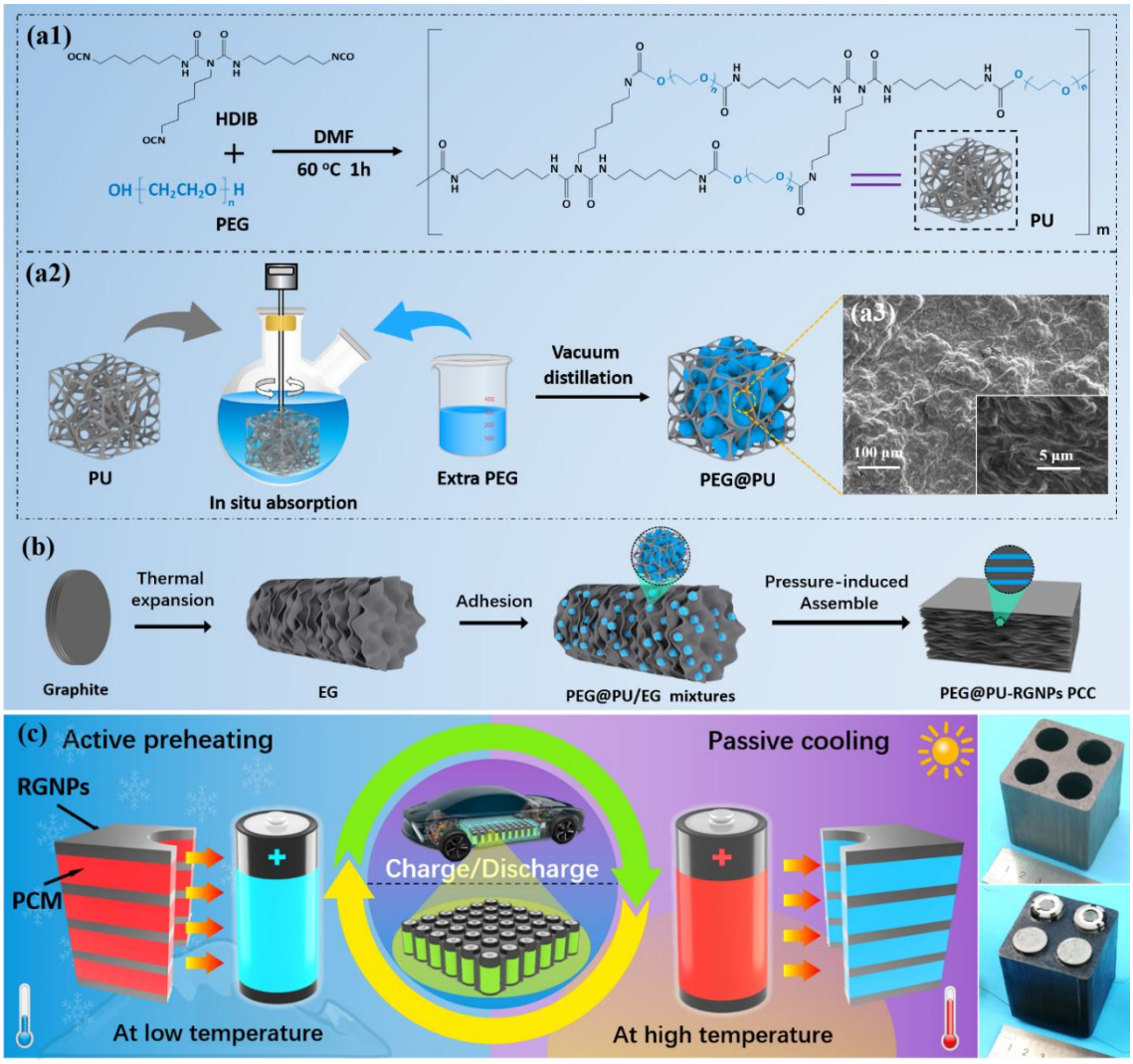

Efficient energy storage and management attracts increasing concerns with the rapid industrial development, energy consumption and growing population.[1] Thermal energy storage (TES) using phase-change materials (PCMs) has been developed as a promising technology to address the mismatch between thermal energy supply and demand.[2,3] Among various PCMs, organic polyethylene glycol (PEG) has drawn tremendous attention owing to its incomparable advantages, including high energy density, thermal and chemical stability, no toxicity, good biocompatibility, and low cost.[4,5] However, as the similar drawbacks of conventional solid-liquid PCMs, the leakage issues during the phase change process greatly restricts the wide application of PEG.[6] To solve this problem, one feasible solution is to modify PEG into polyurethane-based solid-solid PCMs using the chemical crosslinking method.[7,8] The PEG is chemically linked to the supporting material *via* different linkages such as urethane, ester, and ether modification.[9,10] In a typical cross-linked network of polyurethane (PU), PEG serves as a soft phase transition segment, and the hard segment of diisocyanates and chain extenders are responsible for avoiding the free flow of the soft segment during the phase change process. Despite the excellent shape-stabilized property and thermal stability of cross-linked solid-solid PCMs, the chemical or physical bunding of solid-solid PCM restricts the free movement of crystallizable soft parts, which results in the compromise of the thermal energy storage capacity.[11,12]

Apart from the above-mentioned bottlenecks, the low thermal conductivity of pristine PCM is also a great concern for thermal charging/discharging. PEG-based PCMs typically have unsatisfied thermal conductivity ranging from 0.1 to 0.5 W m^{-1} K^{-1},[13] and thus hardly meet the high-power capacity demand.[14] To address this long-standing problem, intensive efforts have been dedicated by introducing high-conductivity fillers into the PCMs.[15] Among various high-conductivity fillers, carbon-based porous

materials, such as graphite/graphene foam (GF),[14,16] carbon aerogel (CA),[17] graphene aerogel (GA),[18,19] carbon nanotube sponge (CNTS)[7,20,21] and expanded graphite (EG)[22,23], are frequently adopted to improve the thermal conductivity of PCMs by fabricating phase change composites (PCCs). Although the components of these porous fillers, such as graphene and carbon nanotube, exhibit ultrahigh intrinsic thermal conductivity (> 1500 W m^{-1} K^{-1} [24]), only modest thermal conductivity enhancement of PCCs has been observed even at a high loading of additives due to the high thermal resistance between conductive fillers and adjacent PCMs.[14,25] Moreover, the unsatisfied thermal and mechanical stability of PCCs can also cause the degeneration of thermal conductivity during the phase transition process.[26] Additionally, the inherent shortcomings of conventional PCCs, such as high cost, low yield, and tedious preparation, hinder their extensive applications.[27] Hence, it is a great challenge to develop high-performance PCCs with high thermal conductivity, excellent thermal properties, and satisfying mechanical stability, for scalable thermal energy storage and management.

Herein, we report a dual-encapsulation strategy to fabricate highly conductive and liquid-free PEG-based PCCs. During the first encapsulation process, the PEG is infiltrated into the cross-linked network of PU to synthesize a highly hybridized semi-interpenetrated composite (PEG@PU). The three-dimensional PU network endows the PEG to alleviate its leakage problem, and the inherent phase change property of PU also improves the thermal storage capacity of the PEG@PU composite. During the secondary encapsulation process, the PEG@PU composites are incorporated with aligned reticulated graphite nanoplatelets (RGNPs) *via* facile pressure-induced assembly strategy to fabricate highly conductive PCCs (PEG@PU-RGNPs). The layer-by-layer RGNPs network enables the PCCs to exhibit high thermal conductivity

(27.0 W m^{-1} K^{-1}) and superior electrical conductivity (51.0 S cm^{-1}) at RGNPs loadings below 30 wt%. Furthermore, we demonstrate the PCC-based energy storage device for battery thermal management (BTM) toward the versatile demands of passive cooling at high temperatures and active warm-up at low temperatures. The operating temperature of a battery pack can be controlled below 55 °C owing to the latent heat of the PCC even at a hot environment (35 °C) during the continuous high-rate charging/discharging cycles. On the other hand, the batteries can be actively preheated by the electro-driven Joule heating of the PCC to maintain a moderate temperature range (35-40 °C) at a low ambient temperature (0 °C), which increases the battery capacity by 13.5% compared with the bare battery pack. Therefore, our work provides a promising route to synthesizing high-performance PCCs for various heat-related energy storage and thermal management for both heating and cooling demand.

Figure 1 shows the schematic illustration of the dual-encapsulation strategy for fabricating highly conductive and liquid-free PEG-based PCCs. During the first encapsulation process (Figure 1a1,a2), one-step polymerization and *in situ* absorption method are adopted to synthesize highly hybridized semi-interpenetrated PEG@PU composite. Typically, a certain amount of PEG and Hexamethylene Diisocyanate Biuret (HDIB) (3:2 molar ratio of PEG/HDIB) are respectively dissolved in *N, N*-Dimethylformamide (DMF) under mechanical stirring at 60 °C and protected with nitrogen. When the solution became sticky, a certain amount of extra PEG is added quickly. The cross-linked polyurethane (PU) network rapidly absorbed the PEG solution. After completion, the composite solution is transferred to a vacuum oven (60 °C) for 24 h to obtain the PEG@PU. The mass fraction of the PEG in the PEG@PU composite is optimized as 70 wt% according to the leakage proof testing (Figure S1).

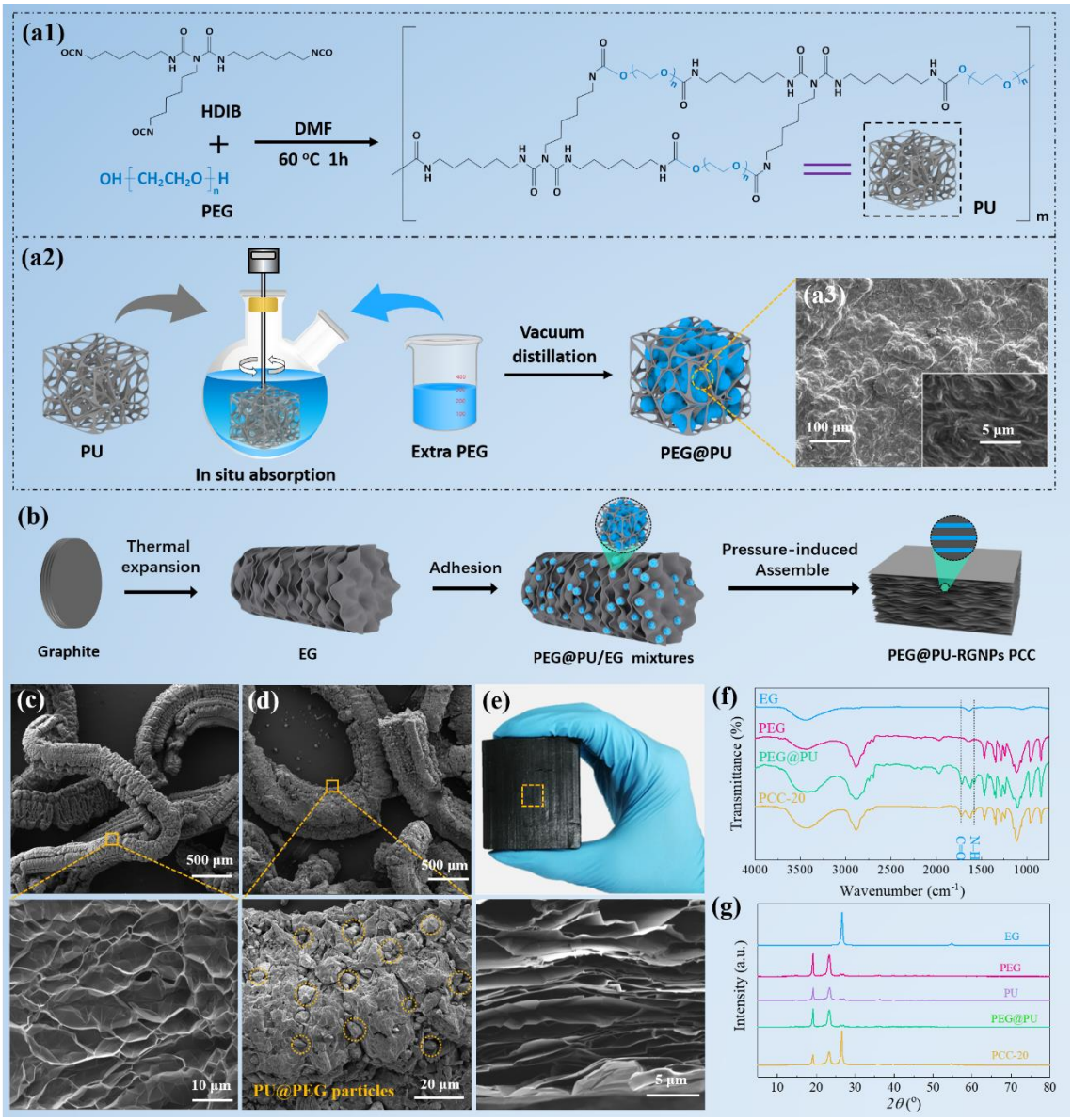

Figure 1. Schematic illustration of a dual-encapsulation strategy for fabricating highly conductive and liquid-free PEG-based PCCs. (a1-a3) The first encapsulation process for synthesizing highly hybridized semi-interpenetrated composites (PEG@PU) by infiltrating PEG into the cross-linked PU network, **(b)** The secondary encapsulation process for preparing highly conductive PEG@PU-RGNPs PCCs by incorporating PEG@PU into RGNPs matrix *via* pressure-induced assembly and the enlarged image showing the microstructure of PEG@PU, **(c)** SEM image of worm-like EG and its enlarged image showing the RGNP networks, **(d)** SEM image of PEG@PU and EG mixtures and its enlarged image showing the PEG@PU particles adhered on the surface of RGNPs, **(e)** Digital photograph of PEG-based PCC block (PEG@PU-RGNPs), and the enlarged cross-section image showing the layer-by-layer aligned RGNPs network after removing the PEG@PU from the PCC, **(f)** Fourier-transform infrared spectroscopy (FT-IR) of EG, PEG, PEG@PU, and PEG@PU-RGNPs, **(g)** X-ray diffraction (XRD) patterns of EG, PEG, PU, PEG@PU, and PEG@PU-RGNPs.

During the second encapsulation process (Figure 1b), a facile pressure-induced assembly method is employed to fabricate highly conductive PEG@PU-RGNPs composites. The pulverized PEG@PU microparticles are mixed with EG at a certain ratio and vigorously stirred and then heated to 120 ºC for approximately 10 min to make the PEG@PU microparticles uniformly adhere to the porous structure of EG. The incompact composites of PEG@PU and EG are then moved into a steel mold and compressed into a shaped composite at 60 ºC under the maximum compression pressure of 20 MPa. The mass fraction of RGNPs in PEG@PU-RGNPs composite is in a range of 5-30 wt% and the as-prepared composites are named as PCC-*x*, where *x* represents the mass fraction of RGNPs.

The microstructures of PEG@PU, EG, and PEG@PU-RGNPs are presented in Figure 1. The cross-section of PEG@PU exhibits a compact structure. Whereas, irregular wrinkled strips are observed in the magnified SEM image of PEG@PU because of the crystallization of PEG segments (Figure 1a3), demonstrating extra PEG is successfully infiltrated and occupied the void space of the 3D cross-linked PU network.[12,28] Figure 1c shows the thermally expanded worm-like EG is composed of numerous disordered RGNPs connected with van-der-Waals interactions. After blending, the PEG@PU microparticles are readily adhered to EG and uniformly distributed on the surface of RGNPs (Figure 1d). For the PCC blocks, a compact layer-by-layer aligned RGNPs network is formed after compression (Figure 1e), which contributes to the anisotropic thermal conductivity of the PCC block. In addition, the XPS spectrum reveals that the RGNPs are highly carbonized, and low oxygen content (1.07 %) is observed after thermal expansion, which contributes to the conductivity enhancement of the PCC (Figure S2).[29]

The FT-IR spectra of PEG, PEG@PU, EG, and PEG@PU-RGNPs are showed in Figure

1f. In the spectrum of PEG, the strong absorption peaks at 2878, 1468, 962, and 840 cm^{-1} are ascribed to C–H bonds, the peaks of –OH stretching vibration, and C–O–C symmetrical vibration appear at 3468 and 1106 cm^{-1}, respectively. The characteristic absorption peaks of HDIB are observed at 3342, 2264, and 1678 cm^{-1}, which are corresponding to the N–H, –NCO, and –NH–CO–NH– stretching vibration, respectively (Figure S3). In the FT-IR spectrum of PEG@PU, after reaction, the peaks of –NCO and –NH–CO–NH– disappeared, while the emergence of new peaks at 1720 and 1533 cm^{-1} are attributed to the stretching vibration of –NHCOO– formed by the polymerization of HDIB and PEG.[30] In addition, the FT-IR spectrum of PEG@PU is similar to PU except for the stretching vibration of –OH at 3464 cm^{-1} of PEG, indicating the infiltration of PEG into the cross-linked PU network. Moreover, no new peaks are observed between spectra of EG, PEG@PU, and PEG@PU-RGNPs, suggesting that the dual-encapsulated PEG@PU-RGNPs is only a physical combination of PEG, PU, and RGNPs.

The crystalline phases of PEG, PU, EG, PEG@PU, and PEG@PU-RGNPs are analyzed by XRD as shown in Figure 1g. The sharp diffraction peaks of pristine PEG at 19.2° and 23.4° are ascribed to the lattice plane of (120) and ($1\bar{3}2$), respectively. In the XRD curves of PU and PEG@PU, almost the same diffraction peaks at around 19.2° and 23.4° are observed as pristine PEG, which reveals that the crystallization property of the PEG in the cross-linked system does not change after polymerization with HDIB. The intensity of diffraction peaks proves that the crystalline regions of PEG in the PU have been decreased to some extent owing to the restriction caused by the crosslinking structure. However, the diffraction intensity of PEG@PU becomes stronger than that of PU, revealing that the crystallinity of PEG increases because of the additional PEG. Moreover, the XRD pattern of the PEG@PU-RGNPs is almost the sum of curves of EG and PEG@PU with a reduction in the intensity for all three peaks, representing the

physical combination of the RGNPs and the PEG@PU. Notably, these results are further validated by the following DSC experiment.

The phase change enthalpies and temperatures of PEG@PU-RGNPs PCCs are characterized by differential scanning calorimetry (DSC). After reacted with HDIB, PU shows an inherent phase change enthalpy (ΔH_m) of 120.6 J g^{-1} and decreased melting temperature (T_m) of 43.4 °C, resulting from chemical restriction and physical entanglements (Table S1).[30] The ΔH_m and T_m of PEG@PU composite raise with the increase of extra PEG loading (Figure S4), and the PEG@PU with 70 wt% PEG loading possesses a ΔH_m of 163.5 J g^{-1} and T_m of 46.5 °C, which is superior to the previously reported PEG-based PCMs with T_m ranges of 35-65 °C (Table S2). Figure 2a presents the DSC results of PCCs and the corresponding data is also summarized in Table S3. After the inclusion of PEG@PU within RGNPs, no significant changes of T_m and freezing temperature (T_c) are observed, demonstrating that the effective physical combination of RGNPs has no significant effect on the melting and crystallization of PEG@PU.[7] However, the phase change enthalpies of PCCs are suppressed as the increase of RGNPs content since RGNPs have no effective phase change behavior at the temperature around 50 °C.

Thermal degradation of PEG@PU and PCCs are measured by TGA which are given in Figure 2b. The detailed data are summarized in Table S4. The thermal degradation of the PEG@PU, PCC-10, PCC-20, and PCC-30 samples all involve two steps. In the first step, about 5% weight loss occurred at the temperature range of 280-360 °C due to the degradation of the urethane segment in the PU molecular chains. The second degradation stage appears in a range from 365 to 430 °C due to the decomposition of PEG.[31] A slight decrease in degradation temperature of maximum weight loss rate is

observed as the RGNPs loading increases. This phenomenon occurs mainly because the thermal conductivity of the PCC is improved as the improvement of RGNPs loading, which promotes the internal heating rate of the PCC. In addition, the amount of char yielding at the maximum temperature for PEG@PU and PCCs are 2.1%, 11.4%, 21.5%, and 31.0%, respectively, which is consistent with the mass fraction of RGNPs in the composites. Notably, no significant degradation occurs below the melting temperature of the PCCs.

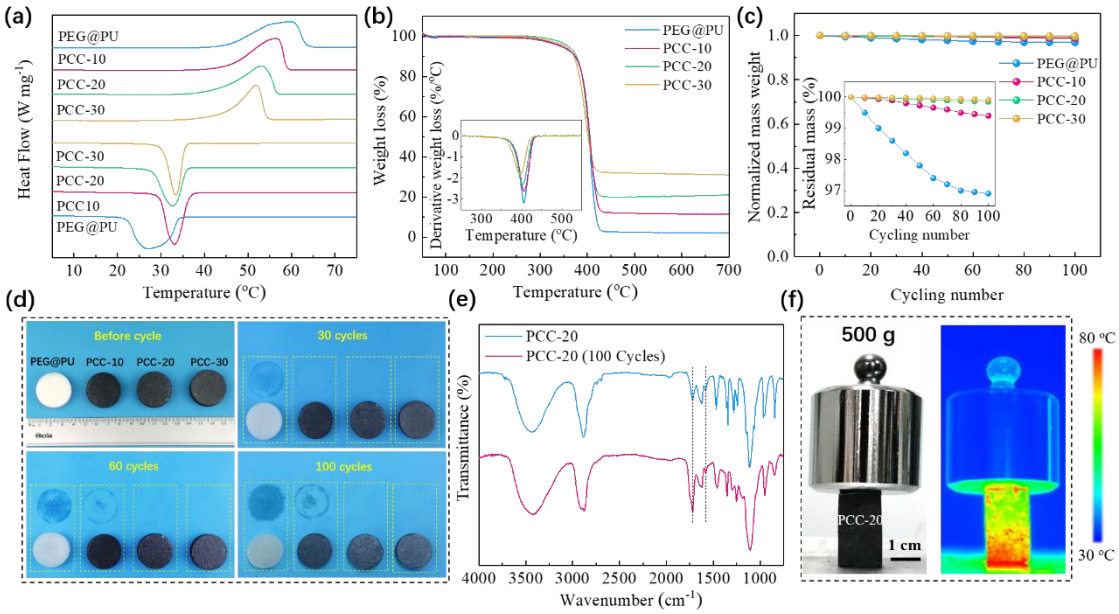

Figure 2. Thermal Performance and Stability of PEG@PU-RGNPs PCCs. (a) The DSC curves of PEG@PU and PEG@PU-RGNPs composites, **(b)** TGA and corresponding DTG curves of PEG@PU and PEG@PU-RGNPs composites, **(c)** The weight loss of PEG@PU and PEG@PU-RGNPs PCCs at different cycling times, **(d)** Digital images of PEG@PU, PCC-10, PCC-20 and PCC-30 during 100 times thermal cycling test, **(e)** FT-IR spectra of PCC-20 before and after 100 thermal cycles, **(f)** Mechanical property test of PCCs, note: the PCC sample was heated on a heating panel with constant temperature of 80 °C.

The thermal stability of the PCC for a long-term operation in a harsh working environment is also examined. Figure 2c,d show the comparison of the weight losses of PEG@PU, PCC-10, PCC-20, and PCC-30 samples during the 100 times endothermic and exothermic cycles under the temperature range of 25-100 °C. The PEG@PU shows

a significant weight loss in the first 60 cycles, while the trend is eased after 80 cycles. The final weight loss of PEG@PU is around 3.1%, indicating the leakage phenomenon of PEG is greatly alleviated after the first encapsulation of PU. Notably, the final weight losses of PCC-10, PCC-20 and PCC-30 are reduced to 0.6%, 0.15% and 0.09%, respectively, demonstrating the successful encapsulation of PEG@PU within RGNPs networks further alleviates the leakage problem of PEG. On the other hand, there is no significant evolution of the phase change enthalpy of PCC-20 during the melting and freezing process (Figure S5,6). Also, the FT-IR spectra of PCC-20 after 100 thermal cycles is highly consistent with the original PCC (Figure 2e), indicating a stable chemical structure of the PCC-20. Moreover, our PCC blocks also demonstrated excellent mechanical property even during the phase transition process (Figure 2f). These results show no significant thermal or chemical degradation occurs during the long-term thermal cycling process, which indicates the excellent thermal stability of PCCs.

Thermal conductivity (K) of PCCs is an important parameter, which determines the thermal power during the charging/discharging process. PEG and PEG@PU have a low thermal conductivity of 0.26-0.35 W m^{-1} K^{-1}, while the PCCs exhibit the anisotropic and highly enhanced thermal conductivities due to the introduction of highly conductive layered RGNPs network as observed by SEM (Figure 3a). Both axial and radial thermal conductivities of PCCs increase with increasing RGNPs loading. Specifically, the PCC-30 shows radial thermal conductivity as high as 27.0 W m^{-1} K^{-1}, which is about 102 times higher than the pristine PEG. The high thermal conductivity enhancement of the resultant PEG@PU-RGNPs composites can be explained by two mechanisms. Firstly, different from conventional preparation methods,[32-35] the inherent large-size RGNPs structure of the EG matrix has maintained to construct large-scale heat transfer

pathways.[36] On the other hand, the interfacial thermal resistance between adjacent RGNPs and PCM in the compact PCCs can be greatly reduced by employing pressure-induced directional compression assemble strategy, which thus boost the transmission of phonons and reduce the overall thermal resistance.[5,23,37] Although many previous results demonstrated that carbon-based additives can enhance the thermal conductivity of PCMs, the thermal conductivity enhancement shows a huge difference even using the same additive and loading content.[7,19,28,38-41] Besides, the fabrication of PCCs with high additive content is still challenging.[42]

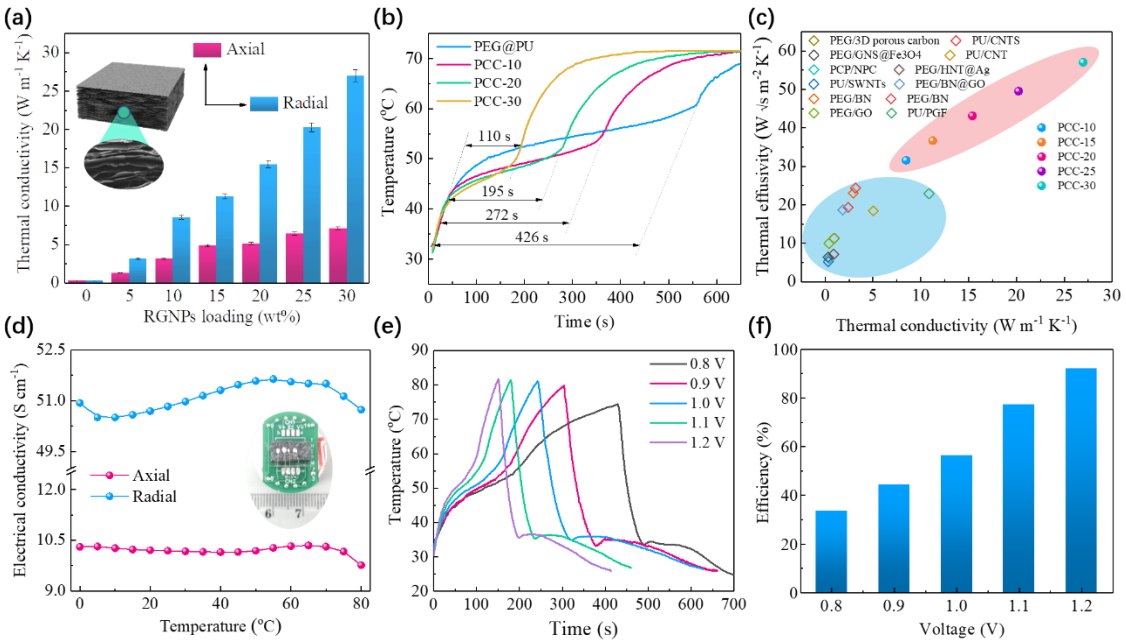

Figure 3. Thermal and electrical conductivities of PEG@PU-RGNPs PCCs. (a) Anisotropic thermal conductivities of PCCs at different RGNPs contents, **(b)** Time-temperature curves of PEG@PU, PCC-10, PCC-20 and PCC-30 samples under a constant heating temperature of 80 °C, **(c)** A comparison of the thermal effusivity and thermal conductivity of PCCs from the latest reports,[7,31,41,44-53] note: some reports did not mention the density of the PCC, thus we calculate the probably maximum thermal effusivity of the PCCs by using the maximum density of the composite block, assuming the PCM and carbon matrix are perfectly mixed and there are no pores existing inside the composite blocks, **(d)** Anisotropic effective electrical conductivity of the PCC-20 at different working temperatures, The inset showing the digital photo of PCC-20 sample for electric conductivity test, **(e)** Time-temperature evolution curves of the PCC-based electro-thermal conversion & storage device during the charging and discharging processes, **(f)** Electro-thermal

conversion efficiencies of the PCC-based electro-thermal conversion & storage device at different voltages.

To further reveal the effect of different thermal conductivities on heat transfer performance of PCCs, transient temperature responses of the PEG@PU and PEG@PU-RGNPs composites are recorded. As shown in Figure 3b, the temperature evolution curves of PEG@PU and PCCs show that the thermal response behavior is more sensitive and the temperature increase becomes faster as the RGNPs loading increases, indicating the combination of RGNPs significantly enhances the heat transfer performance of PCCs. In addition, the infrared images provided in Figure S7 further demonstrate the enhanced heat diffusion capability of the PCCs.

In addition to the thermal conductivity, thermal effusivity (Eq. 1) is another important parameter, which represents the thermal energy exchange capacity of the PCCs.[43]

$$e = \sqrt{K\rho\Delta H} \tag{1}$$

where ρ and ΔH are the bulk density and phase change enthalpy of PCC.

Figure 3c shows the comparison of the thermal effusivities between the as-synthesized PEG@PU-RGNPs composites and the previously reported PEG-based PCCs from the literature.[7,31,41,44-53] As can be seen, our PCCs not only exhibit superior thermal conductivities, but also display higher thermal effusivities, which ensures the high-efficient heat exchange capability (Table S5).

Recently, electro-thermal conversion and storage based on functional PCCs has shown great potential in the thermal energy management of electronic devices, power vehicles, and off-peak electricity storage systems.[15,54-56] The thermal conductivity and electrical conductivity of PCC are two main factors affecting their electro-thermal conversion performance. Figure 3d shows the layered RGNPs not only serve as a highly conductive

matrix but also provide a conductive percolation network to enhance the electrical conductivity of PCCs. Similar to the thermal conductivity, an anisotropic electrical conductivity of PCC-20 is observed, where the radial electrical conductivity (51 S cm^{-1}) is about 4 times higher than the axial one (10 S cm^{-1}) at the temperature range of 0-80 ^{o}C. Subsequently, the PCC-20 samples are subjected to a constant voltage (0.8-1.2 V) along the radial direction to perform electro-thermal conversion and storage. As shown in Figure 3e, the temperatures of PCCs increase rapidly at the initial stage until to a plateau with small slope at T_m of 44 ^{o}C, indicating the generated Joule heat is stored by the latent heat of PCC.[7] After the energy storage is completed, another rapid temperature rise appears and drops sharply when the power supply is cut off. During the natural cooling process, the second temperature plateau at T_c of 35 ^{o}C is associated with the crystallization of PCCs. These values of the phase-change plateau during the electro-driven heating and cooling processes are constant with the DSC results discussed above (Figure 2a and Table 1). Besides, the phase-change duration of the heating plateau is greatly shortened with increasing driving voltage. The electro-thermal conversion efficiency of PCC-20 increases from initially 33.6% to the maximum value of 92.1% as the driving voltage rising to 1.2 V (Figure 3f). The elevation of energy conversion efficiency at higher voltage is mainly attributed to the fact that higher voltage shortens the phase-change duration and thus ultimately suppresses convective and radiative heat losses to the environment.

Considering the superior thermal properties and electro-thermal conversion & storage performance of PEG@PU-RGNPs composite, we further demonstrate the PCC-based energy device for BTM by using commercial 18650 lithium-ion batteries (LiB). Figure 4a shows the concept design of PCC-based BTM for both preheating and cooling demands of LiBs. When the battery is exposed to low-temperature environment, the LiB

is preheated by the Joule heat generated from the electro-thermal conversion of PCC, and the latent heat of PCC during the crystallization process provides a long-time warm-up of the LiBs. By contrast, in a high-temperature environment, the thermal heat released by LiB is absorbed by PCC through its phase transition to maintain an optimum operating temperature, and thus prevent the risks of capacity loss, lifespan shortening, and even thermal runaway of the LiBs.

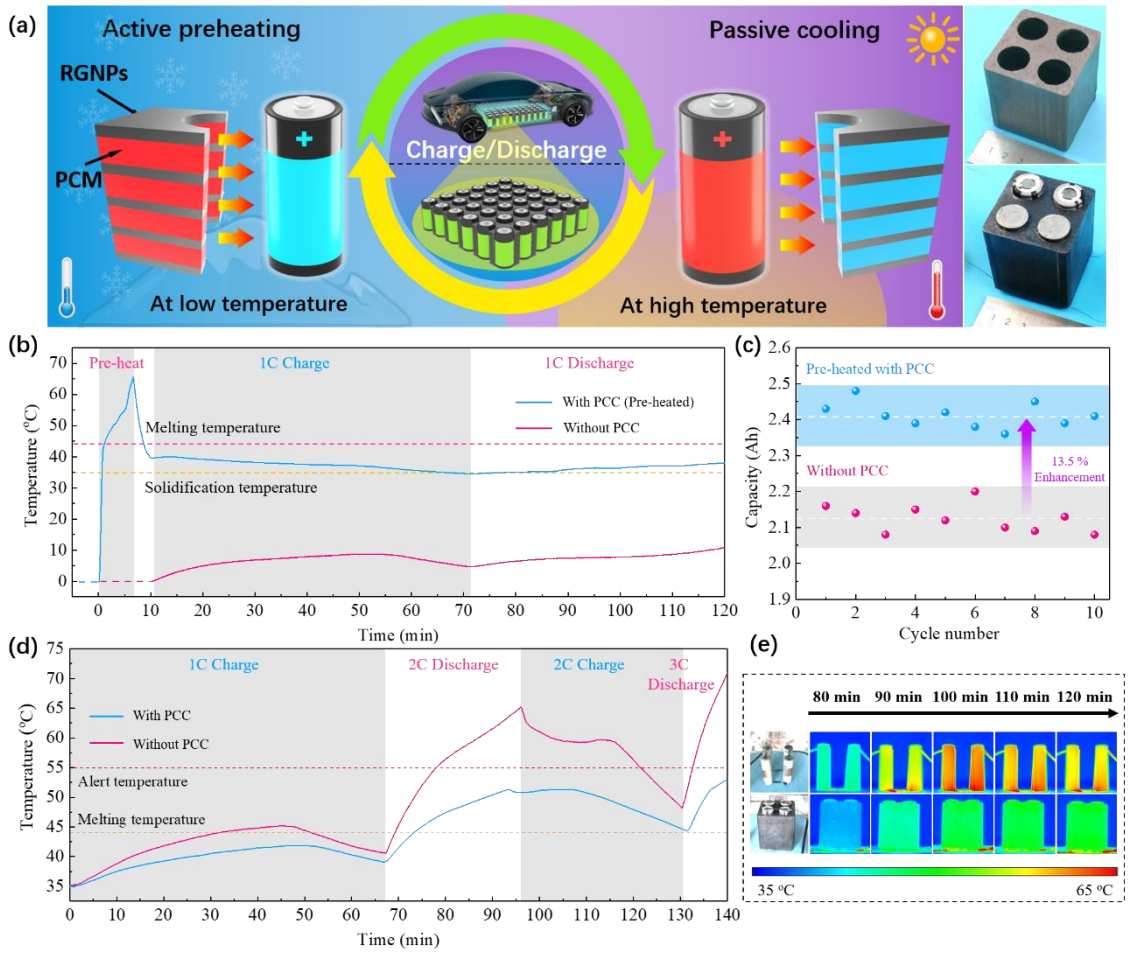

Figure 4. Demonstration of the PCC-based battery thermal management. (a) Schematic of PCC-based electro-driven preheating and passive cooling strategy of batteries and the digital images of LiB pack wrapped with PCC block, **(b)** Comparison of temperature evolution curves of the LiB packs with and without PCC warm-up at a cold environment (0 °C), **(c)** Comparison of the effective energy capacities of the LiB packs with and without PCC-based active warm-up, **(d)** Comparison of temperature evolution curves of the LiB packs with and without PCC cooling at a hot environment (35 °C), **(e)** Digital photos of LiB packs with and without PCC wrap and the corresponding infrared images during charge/discharge process from 80 to 120 min.

To verify the feasibility of the PCC-based BTM under a low-temperature environment, two LiB packs with and without PCC-20 block wrap were tested, among which a certain voltage is applied to electrically preheats the wrapped LiB pack *via* electro-thermal conversion of PCC blocks before initiating the LiB charge/discharge. Figure 4b displays the temperature evolution curves of LiB packs with and without the PCC-based BTM at low ambient temperature (0 ºC). For the PCC-wrapped LiB pack, a sharp temperature rise is observed during the initial period of the electrical-driven preheating process. As the applying voltage continues, the temperature rise slows down at 45 ºC until another sharp temperature slope appears starting from 55 ºC indicating the completion of the phase change process of PCC. After the termination of the electrical preheating process, the temperature of the LiB pack decreases with a relatively high rate resulted from natural cooling until reaching a second plateau with a minimum slope at around 39 °C. The temperature evolution trend of the LiB pack is consistent with the DSC and electro-thermal conversion results of PCCs, and the small difference between T_c and second plateau is mainly caused by the thermal inertia of the PCC block, thus demonstrates that the LiB pack can be effectively preheated by PCC through the electro-thermal conversion. During the successive 1C charge/discharge process, a relatively mild temperature curve is observed at ranges of 34.8-40 ºC. In contrast, the bare LiB pack without warm-up exhibits a more intense temperature change (0-11 ºC) during the continuous charge/discharge process. These results indicate that a stable and optimum working temperature of the LiB pack can be provided through the release of latent heat of PCC in a low-temperature environment. Furthermore, in the past, it was commonly accepted that operating LiBs at high temperatures should be avoided due to the concerns of accelerated degradation and possible thermal runaway. However, recent studies revealed that preheating LiBs at the charging stage *via* finite exposure to an

elevated temperature can remarkably improve the rate capability and cycle life, especially from a cold start.[57-59] As a result, the effective charge capacity of the LiB pack with active preheating of PCC wrap is improved by 13.5% compared with the bare LiB pack after 10 cycles at 0 ºC (Figure 4c).

In addition to the active warm-up of the LiB pack in a cold environment, the passive cooling performance of PCC is also examined. During the passive cooling test, two LiB packs with and without PCC wrap are adopted to perform consecutive charge/discharge at the temperature of 35 ºC. As illustrated in Figure 4d, two LiB packs show similar temperature evolution trends. However, the temperature of PCC-wrapped LiB is far lower than that of nonwrapped one, especially during the high charge/discharge current. For example, the maximum temperatures of bare LiB reach 65 ºC and even 70 ºC under 2C and 3C discharge processes, while that of wrapped LiB pack remains lower than the alarming temperature (55 ºC) at high charge/discharge process. This is mainly because of the high thermal conductivity and thermal energy storage capacity of the PCC wrap, where the heat generated from LiB rapidly transfers to the internal RGNPs and is stored in PCC. Moreover, compared with the bare LiB pack, the infrared images of the wrapped pack exhibited a uniform temperature distribution, which further demonstrates the superior cooling performance of PCC (Figure 4e)

In conclusion, a dual-encapsulation strategy is reported to fabricate highly conductive and liquid-free PEG-based PCCs for thermal management by introducing the cross-linked network of PU and the layer-by-layer network of RGNPs into PEG. After the impregnation of PEG into the 3D PU network, the leakage of PEG is greatly alleviated and the resultant highly hybridized PEG@PU exhibits an enlarged latent heat of 163.5 J g^{-1}. The introduction of the aligned layer-by-layer network of RGNPs not only further improves the thermal and durable stabilities of PCCs, but also results in

tailored thermal conductivities of 3.1-27.0 W $m^{-1} K^{-1}$ at RGNPs loadings of 5-30 wt%. Meanwhile, the resultant PCC also exhibits superior electrical conductivity (51.0 S cm^{-1}) and efficient electro-thermal conversion and storage (~92.1%) under a low applying voltage of 1.2 V. Consequently, the PCC-based BTM shows that a moderate working temperature range can be provided through active electro-driven preheating or passive cooling of PCC under cold or hot environment during a continuous charge/discharge process. Therefore, our works provide a route of synthesizing high-performance PCCs and pave a way for the versatile thermal management of electronics toward both warm-up and cooling demands.

ASSOCIATED CONTENT

Supporting Information. The Supporting Information is available free of charge at https://pubs.acs.org/. This material includes materials preparation, characterizations, thermal performance comparison and experimental details.

AUTHOR INFORMATION

Correspondence Authors

Tingxian Li - Research Center of Solar Power & Refrigeration, School of Mechanical Engineering, Shanghai Jiao Tong University, Shanghai, 200240, China; orcid.org/0000-0003-4618-8144; Email: Litx@sjtu.edu.cn

Ruzhu Wang - Research Center of Solar Power & Refrigeration, School of Mechanical Engineering, Shanghai Jiao Tong University, Shanghai, 200240, China; orcid.org/0000-0003-3586-5728; Email: Rzwang@sjtu.edu.cn

Authors

Minqiang Wu - Research Center of Solar Power & Refrigeration, School of Mechanical Engineering, Shanghai Jiao Tong University, Shanghai, 200240, China; orcid.org/0000-0001-9497-8015

Pengfei Wang - Research Center of Solar Power & Refrigeration, School of Mechanical Engineering, Shanghai Jiao Tong University, Shanghai, 200240, China;

Si Wu - Research Center of Solar Power & Refrigeration, School of Mechanical Engineering, Shanghai Jiao Tong University, Shanghai, 200240, China; orcid.org/0000-0002-8548-431X

Taisen Yan - Research Center of Solar Power & Refrigeration, School of Mechanical Engineering, Shanghai Jiao Tong University, Shanghai, 200240, China; orcid.org/0000-0001-6623-0974

Jiaxing Xu - Research Center of Solar Power & Refrigeration, School of Mechanical Engineering, Shanghai Jiao Tong University, Shanghai, 200240, China; orcid.org/0000-0002-8913-9783

Jie Lin - Department of Engineering Science, University of Oxford, Parks Road, Oxford OX1 3PJ, United Kingdom; orcid.org/0000-0003-3323-2089

Author Contributions

M. Wu and T. Li contributed equally to this work.

Notes

The authors declare no competing financial interest.

ACKNOWLEDGMENT

This work was supported by the National Natural Science Foundation of China (No.51876117) and the National Key R&D Program of China (No.2018YFE0100300). Part of this work was funded by the Innovative Research Groups of National Natural Science Foundation of China (No.51521004).

REFERENCES

1. Tilman, D., R. Socolow, J.A. Foley, et al., *Beneficial biofuels—the food, energy, and environment trilemma.* Science, 2009. **325**(5938): p. 270-271.

2. Liu, C., F. Li, L.P. Ma, et al., *Advanced materials for energy storage.* Advanced materials, 2010. **22**(8): p. E28-E62.

3. Liu, C., Z. Rao, J. Zhao, et al., *Review on nanoencapsulated phase change materials: preparation, characterization and heat transfer enhancement.* Nano Energy, 2015. **13**: p. 814-826.

4. Rathod, M.K. and J. Banerjee, *Thermal stability of phase change materials used in latent heat energy storage systems: A review.* Renewable and sustainable energy reviews, 2013. **18**: p. 246-258.

5. Wu, S., T. Yan, Z. Kuai, et al., *Thermal conductivity enhancement on phase change materials for thermal energy storage: A review.* Energy Storage Materials, 2020. **25**: p. 251-295.

6. Ahmadi, Y., K.H. Kim, S. Kim, et al., *Recent advances in polyurethanes as efficient media for thermal energy storage.* Energy Storage Materials, 2020. **30**.

7. Aftab, W., A. Mahmood, W. Guo, et al., *Polyurethane-based flexible and conductive phase change composites for energy conversion and storage.* Energy Storage Materials, 2019. **20**: p. 401-409.

8. Qian, T., J. Li, X. Min, et al., *Enhanced thermal conductivity of PEG/diatomite shape-stabilized phase change materials with Ag nanoparticles for thermal energy storage.* Journal of Materials Chemistry A, 2015. **3**(16): p. 8526-8536.

9. Sundararajan, S., A.B. Samui, and P.S. Kulkarni, *Versatility of polyethylene glycol (PEG) in designing solid-solid phase change materials (PCMs) for thermal management and their application to innovative technologies.* Journal of Materials Chemistry A: p. 10.1039.C7TA04968D.

10. Ahmadi, Y., K.-H. Kim, S. Kim, et al., *Recent advances in polyurethanes as efficient media for thermal energy storage.* Energy Storage Materials, 2020.

11. Zhou, Y., X. Wang, X. Liu, et al., *Polyurethane-based solid-solid phase change materials with halloysite nanotubes-hybrid graphene aerogels for efficient light- and electro-thermal conversion and storage.* Carbon, 2018.

12. Zhang, Y., L. Wang, B. Tang, et al., *Form-stable phase change materials with high phase change enthalpy from the composite of paraffin and cross-linking phase change structure.* Applied energy, 2016. **184**: p. 241-246.

13. Sundararajan, S., A.B. Samui, and P.S. Kulkarni, *Versatility of polyethylene glycol (PEG) in designing solid–solid phase change materials (PCMs) for thermal management and their application to innovative technologies.* Journal of Materials Chemistry A, 2017. **5**(35): p. 18379-18396.

14. Ji, H., D.P. Sellan, M.T. Pettes, et al., *Enhanced thermal conductivity of phase change materials with ultrathin-graphite foams for thermal energy storage.* Energy & Environmental Science, 2014. **7**(3): p. 1185-1192.

15. Yuan, K., J. Shi, W. Aftab, et al., *Engineering the Thermal Conductivity of Functional Phase‐Change Materials for Heat Energy Conversion, Storage, and Utilization.* Advanced Functional Materials, 2020. **30**(8): p. 1904228.

16. Yang, J., G.-Q. Qi, R.-Y. Bao, et al., *Hybridizing graphene aerogel into three-dimensional graphene foam for high-performance composite phase change materials.* Energy Storage Materials, 2018. **13**: p. 88-95.

17. Huang, X., W. Xia, and R. Zou, *Nanoconfinement of phase change materials within carbon aerogels: phase transition behaviours and photo-to-thermal energy storage.* Journal of Materials Chemistry A, 2014. **2**(47): p. 19963-19968.

18. Mu, B. and M. Li, *Fabrication and thermal properties of tetradecanol/graphene aerogel form-stable composite phase change materials.* Scientific reports, 2018. **8**(1): p. 1-14.

19. Min, P., J. Liu, X. Li, et al., *Thermally Conductive Phase Change Composites Featuring Anisotropic Graphene Aerogels for Real‐Time and Fast‐Charging Solar‐Thermal Energy Conversion.* Advanced Functional Materials, 2018. **28**(51): p. 1805365.

20. Chen, L., R. Zou, W. Xia, et al., *Electro-and photodriven phase change composites based on wax-infiltrated carbon nanotube sponges.* ACS nano, 2012. **6**(12): p. 10884-10892.

21. Zheng, Z., J. Jin, G.-K. Xu, et al., *Highly stable and conductive microcapsules for enhancement of joule heating performance.* ACS nano, 2016. **10**(4): p. 4695-4703.

22. Xia, L., P. Zhang, and R. Wang, *Preparation and thermal characterization of expanded graphite/paraffin composite phase change material.* Carbon, 2010. **48**(9): p. 2538-2548.

23. Wu, S., T. Li, Z. Tong, et al., *High‐Performance Thermally Conductive Phase Change Composites by Large‐Size Oriented Graphite Sheets for Scalable Thermal Energy Harvesting.* Advanced Materials, 2019. **31**(49): p. 1905099.

24. Balandin, A.A., *Thermal properties of graphene and nanostructured carbon materials.* Nature materials, 2011. **10**(8): p. 569-581.

25. Shtein, M., R. Nadiv, M. Buzaglo, et al., *Thermally conductive graphene-polymer composites: size, percolation, and synergy effects.* Chemistry of Materials, 2015. **27**(6): p. 2100-2106.

26. Zheng, R., J. Gao, J. Wang, et al., *Reversible temperature regulation of electrical and thermal conductivity using liquid-solid phase transtions.* Nature Communications, 2011. **2**(1): p. 289.

27. Xiao, C., H. Gao, Y. Mu, et al., *Highly Graphitized 3D Network Carbon for Shape-stabilized Composite PCMs with Superior Thermal Energy Harvesting.* Nano Energy, 2018.

28. Zhou, Y., X. Wang, X. Liu, et al., *Polyurethane-based solid-solid phase change materials with halloysite nanotubes-hybrid graphene aerogels for efficient light-and electro-thermal conversion and storage.* Carbon, 2019. **142**: p. 558-566.

29. Dai, W., T. Ma, Q. Yan, et al., *Metal-level thermally conductive yet soft graphene thermal interface materials.* ACS nano, 2019. **13**(10): p. 11561-11571.

30. Zhou, Y., X. Liu, D. Sheng, et al., *Polyurethane-based solid-solid phase change materials with in situ reduced graphene oxide for light-thermal energy conversion and storage.* Chemical Engineering Journal, 2018. **338**: p. 117-125.

31. Wang, Y., B. Tang, and S. Zhang, *Single‐walled carbon nanotube/phase change material composites: sunlight‐driven, reversible, form‐stable phase transitions for solar thermal energy storage.* Advanced Functional Materials, 2013. **23**(35): p. 4354-4360.

32. Buzaglo, M., I.P. Bar, M. Varenik, et al., *Graphite‐to‐Graphene: Total*

Conversion. Advanced Materials, 2017. **29**(8): p. 1603528.

33. Wang, F., J. Yi, Y. Wang, et al., *Graphite intercalation compounds (GICs): a new type of promising anode material for lithium‐ion batteries.* Advanced Energy Materials, 2014. **4**(2): p. 1300600.

34. Zhang, Z., G. Alva, M. Gu, et al., *Experimental investigation on n–octadecane/polystyrene/expanded graphite composites as form–stable thermal energy storage materials.* Energy, 2018. **157**: p. 625-632.

35. Li, W.-W., W.-L. Cheng, B. Xie, et al., *Thermal sensitive flexible phase change materials with high thermal conductivity for thermal energy storage.* Energy Conversion and Management, 2017. **149**: p. 1-12.

36. Yang, J., Y. Yang, S.W. Waltermire, et al., *Enhanced and switchable nanoscale thermal conduction due to van der Waals interfaces.* Nature nanotechnology, 2012. **7**(2): p. 91-95.

37. Wu, M., T. Li, S. Wu, et al., *Highly Conductive Phase Change Composites Enabled by Vertically-Aligned Reticulated Graphite Nanoplatelets for High-Temperature Solar Photo/Electro-Thermal Energy Conversion, Harvesting and Storage.* Nano Energy, 2021: p. 106338.

38. Mehrali, M., S.T. Latibari, M. Mehrali, et al., *Preparation and characterization of palmitic acid/graphene nanoplatelets composite with remarkable thermal conductivity as a novel shape-stabilized phase change material.* Applied Thermal Engineering, 2013. **61**(2): p. 633-640.

39. Kholmanov, I., J. Kim, E. Ou, et al., *Continuous carbon nanotube–ultrathin graphite hybrid foams for increased thermal conductivity and suppressed subcooling in composite phase change materials.* ACS nano, 2015. **9**(12): p. 11699-11707.

40. Wang, S., P. Qin, X. Fang, et al., *A novel sebacic acid/expanded graphite composite phase change material for solar thermal medium-temperature applications.* Solar Energy, 2014. **99**: p. 283-290.

41. Lv, Y., W. Zhou, and W. Jin, *Experimental and numerical study on thermal energy storage of polyethylene glycol/expanded graphite composite phase change material.* Energy and Buildings, 2016. **111**: p. 242-252.

42. Wu, S., T. Li, M. Wu, et al., *Highly thermally conductive and flexible phase change composites enabled by polymer/graphite nanoplatelet-based dual networks for efficient thermal management.* Journal of Materials Chemistry A, 2020.

43. *A thermal energy storage composite with sensing function and its thermal conductivity and thermal effusivity enhancement.* Journal of Materials Chemistry A, 2019. **7**.

44. Wu, W., X. Huang, K. Li, et al., *A functional form-stable phase change composite with high efficiency electro-to-thermal energy conversion.* Applied Energy, 2017. **190**: p. 474-480.

45. Shi, J., W. Aftab, Z. Liang, et al., *Tuning the flexibility and thermal storage capacity of solid–solid phase change materials towards wearable applications.* Journal of Materials Chemistry A, 2020. **8**(38): p. 20133-20140.

46. Atinafu, D.G., W. Dong, X. Huang, et al., *One-pot synthesis of light-driven polymeric composite phase change materials based on N-doped porous carbon for enhanced latent heat storage capacity and thermal conductivity.* Solar Energy Materials and Solar Cells, 2018. **179**: p. 392-400.

47. Song, S., F. Qiu, W. Zhu, et al., *Polyethylene glycol/halloysite@ Ag nanocomposite PCM for thermal energy storage: Simultaneously high latent*

heat and enhanced thermal conductivity. Solar Energy Materials and Solar Cells, 2019. **193**: p. 237-245.

48. Chen, X., H. Gao, M. Yang, et al., *Highly graphitized 3D network carbon for shape-stabilized composite PCMs with superior thermal energy harvesting.* Nano energy, 2018. **49**: p. 86-94.

49. Liu, D., C. Lei, K. Wu, et al., *A Multidirectionally Thermoconductive Phase Change Material Enables High and Durable Electricity via Real-Environment Solar–Thermal–Electric Conversion.* ACS nano, 2020. **14**(11): p. 15738-15747.

50. Yang, J., L.-S. Tang, R.-Y. Bao, et al., *An ice-templated assembly strategy to construct graphene oxide/boron nitride hybrid porous scaffolds in phase change materials with enhanced thermal conductivity and shape stability for light–thermal–electric energy conversion.* Journal of Materials Chemistry A, 2016. **4**(48): p. 18841-18851.

51. Qiu, J., X. Fan, Y. Shi, et al., *PEG/3D graphene oxide network form-stable phase change materials with ultrahigh filler content.* Journal of Materials Chemistry A, 2019. **7**(37): p. 21371-21377.

52. Wang, W., B. Tang, B. Ju, et al., *Fe 3 O 4-functionalized graphene nanosheet embedded phase change material composites: efficient magnetic-and sunlight-driven energy conversion and storage.* Journal of Materials Chemistry A, 2017. **5**(3): p. 958-968.

53. Yang, J., L.-S. Tang, L. Bai, et al., *Photodriven shape-stabilized phase change materials with optimized thermal conductivity by tailoring the microstructure of hierarchically ordered hybrid porous scaffolds.* ACS Sustainable Chemistry & Engineering, 2018. **6**(5): p. 6761-6770.

54. Chen, X., Z. Tang, H. Gao, et al., *Phase Change Materials for Electro-Thermal*

Conversion and Storage: From Fundamental Understanding to Engineering Design. Iscience, 2020: p. 101208.

55. Gao, H., J. Wang, X. Chen, et al., *Nanoconfinement effects on thermal properties of nanoporous shape-stabilized composite PCMs: A review.* Nano Energy, 2018. **53**: p. 769-797.

56. Zhang, Y., M.M. Umair, S. Zhang, et al., *Phase change materials for electron-triggered energy conversion and storage: a review.* Journal of Materials Chemistry A, 2019. **7**(39): p. 22218-22228.

57. Wang, C.-Y., G. Zhang, S. Ge, et al., *Lithium-ion battery structure that self-heats at low temperatures.* Nature, 2016. **529**(7587): p. 515-518.

58. Yang, X.-G., T. Liu, Y. Gao, et al., *Asymmetric temperature modulation for extreme fast charging of lithium-ion batteries.* Joule, 2019. **3**(12): p. 3002-3019.

59. Hu, X., Y. Zheng, D.A. Howey, et al., *Battery warm-up methodologies at subzero temperatures for automotive applications: Recent advances and perspectives.* Progress in Energy and Combustion Science, 2020. **77**: p. 100806.